Sixth International Symposium on Turbulence and Shear Flow Phenomena
Seoul, Korea, 22-24 June 2009

WAVELET-DECOMPOSED THREE VORTICITY COMPONENTS IN A TURBULENT NEAR WAKE

Akira Rinoshika
Department of Mechanical Systems Engineering,
Yamagata University
4-3-16 Jonan, Yonezawa-shi, Yamagata 992-8510, Japan
rinosika@yz.yamagata-u.ac.jp

Tongming Zhou
School of Civil and Resource Engineering,
The University of Western Australia
35 Stirling Highway, Crawley, WA6009, Western Australia, Australia
tzhou@civil.uwa.edu.au

Yu Zhou
Department of Mechanical Engineering,
The Hong Kong Polytechnic University
Hung Hom, Kowloon, Hong Kong, China
mmyzhou@polyu.edu.hk

ABSTRACT

The purpose of the present study is to examine the characteristics of the vortical structures using the orthogonal wavelet multi-resolution technique by decomposing the vorticity into a number of wavelet components based on different central frequencies. The three vorticity components were measured simultaneously using an eight-wire probe in the near wake of a circular cylinder at three Reynolds numbers, namely 1,600, 6,500 and 10,000. It is found that the dominant contributions to the vorticity variances are from the intermediate and relatively small-scale structures. The contributions from the large and intermediate-scale structures to the vorticity variances decrease with the increase of Reynolds number, while the contributions from the small-scale structures to all three vorticity variances jump significantly, which is connected to previous observations in the near wake that there is a significant increase in the generation of small-scale structures. The result reinforces the conception that turbulence 'remembers' its origin.

INTRODUCTION

Flow around a circular cylinder is of significant importance for engineering applications. The topology and transport characteristics of the turbulent structure in the wake that depend on the initial conditions have been well established studied. Especially the Reynolds number has a significant effect on the formation of vortices behind the circular cylinder and attracted a large amount of investigation in the past several decades particularly in the range of Re = 1,000 to 10,000 (Lin et al., 1995). Recently, Yiu et al. (2004) examined the Reynolds number effects on the turbulent near wake over the Re range of 2,500 – 10,000 using a 4-X-wire 3-dimentional vorticity probe. They found that the streamwise vorticity component "jump" significantly as Re is increased from 5,000 to 10,000. Correspondingly, the contributions from the large-scale structures to the spanwise vorticity variance decline appreciably, suggesting an increased 3-dimentionality of the flow. However, due to the limitation of their detection scheme, they could not provide any information on the relationship between initial conditions and organized structures other than the large-scale ones. One interesting question to be asked is how these variations with *Re* would affect the contribution of various scales to the three-dimensional vorticity in the near wake. This motivates the present investigation.

In the past decade there has been a growing interest in the use of wavelet analysis for extracting new information on the turbulence structures of various scales. Recently, an orthogonal wavelet multi-resolution technique was applied to the analysis of the turbulent structures of various scales in the near-wake of a circular cylinder by Rinoshika and Zhou (2005). It is observed for the first time that the spanwise vorticity contours of the wavelet component at the averaging frequency of Kármán vortices display a secondary spanwise structure near the saddle point in the near wake of a circular cylinder. Using the same technique, Rinoshika & Zhou (2005, 2007) further investigate the dependence of the turbulent structures of various scales on various wake-generating bodies in the near and far wakes. Their results indicate that the intermediate- as well as the large-scale structures depend on the initial conditions.

One objective of this work is to explore further the possible dependence of the near-wake turbulence on Re, in particular, focusing on the aspects of vorticity. For this purpose, a probe that used by Zhou et al. (2006) was employed to measure the three-dimensional vorticity components of far wake simultaneously at two Reynolds

numbers, namely 6,500 and 10,000. Vorticity is an important characteristic of turbulence that can provide fundamental information on multi-scale turbulent structures. Therefore, the second objective is to investigate the connection between the three-component vorticity and the multi-scale vortical structures, which is fundamentally important to the thorough understanding of the near-wake turbulence.

In the present study, the wavelet transform is used to decompose the measured three-component vorticity signals into a number of wavelet components based on their central frequencies, which are representative of the turbulent structures of different scales. The contributions from the turbulent structures of various scales to the vorticity variances are calculated. The Re dependence of large-, intermediate- and small-scale structures is documented in details in terms of the three-dimensional vorticity.

EXPERIMENTAL DETAILS

The experiments were conducted in a closed loop wind tunnel with a test section of 1.2 m (width) × 0.8 m (height) and 2.4 m (length). Across the tunnel, the free-stream flow was uniform within 0.5%. The free-stream turbulence intensity was not more than 0.5%.

Three stainless steel circular cylinders with diameters of d = 6.35, 12.7 and 12.75 mm were used to generate respectively wakes of three free stream velocities, i.e. 4 m/s, 8 m/s and 12 m/s, corresponding to Re ($\equiv U_1 d/\nu$) = 1,600, 6,500 and 10,000, respectively. Table 1 summarizes the characteristic parameters of the wakes. The three velocity components u_1, u_2 and u_3 were measured at the downstream location x/d = 40.

The probe used to measure the three velocity components is sketched in Figure 1. It consists of 4 standard X-probes with X-probes I and III being used to measure u_1 and u_3 at two locations separated by a finite distance Δx_2 = 2.7mm while X-probes II and IV are used to measure u_1 and u_2 at two locations separated by a finite distance Δx_3 = 2.7mm. In the present study, the coordinate system is defined such that the x_1-axis is in the incoming flow of velocity direction, the x_2-axis direction is perpendicular to the x_1-axis in the vertical plane through the cylinder while the x_3-axis is normal to the both x and y axes. The separation between the inclined wires of each X-probe was about 0.6mm. The 2.5μm diameter hot wires were etched from Wollaston (Pt-10% Rh) wires to an active length about 0.5mm, which corresponds to about 200 times wire diameter. The wires were operated on in-house constant temperature circuits at an overheat ratio = 0.5. The wires were calibrated for velocity and inclination angle using a Pitot-static tube connected to a MKS Baratron pressure transducer (least count = 0.01mm H_2O) at the centerline of the tunnel while the angle calibration was performed over ±20° both before and after the experiments to ensure high quality of the data. The included angle of each X-wire was about 110° and the effective angle of the inclined wires, β was about 35°. The output signals comes from the anemometers were passed through buck and gain circuits and low-pass filtered at a cut-off frequency f_c = 5200 Hz which is high enough to examine the vortex shedding frequency but slightly small to examine the small scales of turbulent for vorticity measurements. The filtered signals were subsequently sampled at a frequency f_s = 10400 Hz by using a 16 bit A/D converter. The duration of each record was about 60 seconds. The experimental uncertainty in $\overline{U}$ was estimated to be about ±2% while the uncertainties in u' (or v' and w') were about ± 7%, ± 8% and ± 8%, respectively.

The three vorticity components at x_1, x_2 and x_3 directions are computed based on the measured velocity signals u_1, u_2 and u_3 at different locations, viz.

$$\omega_1 = \frac{\partial u_3}{\partial x_2} - \frac{\partial u_2}{\partial x_3} \approx \frac{\Delta u_3}{\Delta x_2} - \frac{\Delta u_2}{\Delta x_3}, \quad (1)$$

$$\omega_2 = \frac{\partial u_1}{\partial x_3} - \frac{\partial u_3}{\partial x_1} \approx \frac{\Delta u_1}{\Delta x_3} - \frac{\Delta u_3}{\Delta x_1}, \quad (2)$$

$$\omega_3 = \frac{\partial u_2}{\partial x_1} - \frac{\partial (\overline{U} + u_1)}{\partial x_2} = \frac{\Delta u_2}{\Delta x_1} - \frac{\Delta (\overline{U} + u_1)}{\Delta x_2}, \quad (3)$$

where Δu_3 and Δu_1 in (1) and (3), respectively are velocity

Table 1. Summary of the experimental conditions

Re	U_1 (m/s)	d (mm)	U_0 (m/s)	L (mm)
1,600	4	6.35	0.48	5
6,500	8	12.7	0.88	9
10,000	12	12.75	2.13	21

Reynolds number Re≡$U_1 d/\nu$ U_1 is the free stream velocity
d is the diameter of the cylinder
U_0 is the maximum velocity deficit of the wake
L is the half-width of the wake

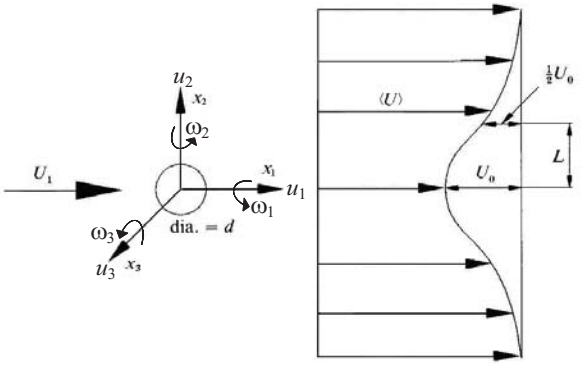

(a) Definition sketches of the flow and coordinate system

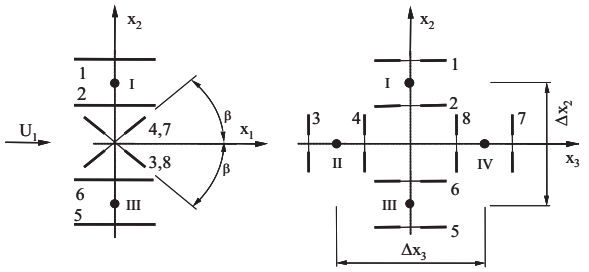

(a) Side view of the probe (b) Front view of the probe

Figure 1 The definition of the coordinate system and the sketches of the vorticity probe.

differences between X-probe I and III (Figure 1b, c); Δu_2 and Δu_1 in (1) and (2), respectively are velocity differences between X-probe II and IV. The spatial separation Δx_1 is estimated based on Taylor's hypothesis, given by $U_c(2\Delta t)$ where U_c= $0.87U_1$ is the average convection velocity of vortices and Δt=$1/f_s$ is the time interval between two consecutive points in the time series of velocity signals.

ORTHOGONAL WAVELET MULTI-RESOLUTION ANALYSIS

Orthogonal wavelet transform and multi-resolution analysis are described in detail in many references and are therefore briefly discussed in this section using matrix operation instead of convectional integral operation.

One-dimensional discrete wavelet transform is a linear and orthogonal transform and is defined in matrix form by

$$\boldsymbol{S} = \boldsymbol{W}\boldsymbol{V}, \tag{4}$$

where $\boldsymbol{V}$ is an one-dimensional data matrix, viz.

$$\boldsymbol{V} = \begin{bmatrix} v_1 & v_2 & . & . & . & v_N \end{bmatrix}^T, \tag{5}$$

$\boldsymbol{S}$ and $\boldsymbol{W}$ are called discrete wavelet coefficient (or spectrum) matrix and analysing wavelet matrix of $\boldsymbol{V}$, respectively. The superscript T in (5) denotes a transposed matrix. $\boldsymbol{W}$ is orthogonal and satisfies $\boldsymbol{W}^T\boldsymbol{W} = \boldsymbol{I}$, where $\boldsymbol{I}$ is a unit matrix. $\boldsymbol{W}$ is usually constructed based on a cascade algorithm of an orthogonal wavelet basis function. In the present study, the Daubechies wavelet basis with an order of 20 is used since the wavelet basis of a higher order has good frequency localization, which in turn increases the energy compaction (Rinoshika, 2005).

Both the analysing wavelet matrix and wavelet basis are orthogonal, implying that the discrete wavelet transform has the inverse transform. One simply reverses the procedure, starting with the smallest level of the hierarch and working from right to left, and the inverse discrete wavelet transform is given by

$$\boldsymbol{V} = \boldsymbol{W}^T\boldsymbol{S}. \tag{6}$$

The discrete wavelet coefficient may be interpreted as the relative local contribution of various scales to the original data. In order to decompose the data into the grouped frequency components, the inverse wavelet transform is applied to the discrete wavelet coefficients at each grouped frequency. This decomposition method is called the wavelet multi-resolution analysis. Hence, Eq. (6) can be rewritten as

$$V = \sum_{i=1}^{N} W^T S_i \,. \tag{7}$$

On the right side of Eq. (7), the first term $\boldsymbol{W}^T\boldsymbol{S_1}$ and the last term $\boldsymbol{W}^T\boldsymbol{S_N}$ represent the wavelet components at wavelet level 1 (the lowest frequency) and level N (the highest frequency).

It is worthwhile remarking that, compared with conventional band-pass filtering techniques, the wavelet components of the discrete wavelet transform are orthogonal to, and hence independent of, each other and do not contain redundant information. This advantage makes the interpretation of the phenomena more reliable.

To extract various scales in turbulence structures, the wavelet multi-resolution analysis is used to decompose the vorticity fluctuation components ω_k into a number of orthogonal wavelet components based on wavelet levels, which correspond to the different central frequencies and are directly linked to turbulent structure scales. The wavelet multi-resolution analysis may process fewer data by selecting relevant details that are essential to perform the extraction of multi-scale flow structures, and decompose the velocity fluctuations both in Fourier and physical spaces. Each wavelet component represents the turbulent structures of a certain range of frequencies so that the information of any scales contained in the original data will not be lost due to a limited number of wavelet levels. The ω_k can be written as

$$\omega_k = \sum_{i=1}^{N} \omega_{k,i} \,, \tag{8}$$

where N is the total number of wavelet levels, and $\omega_{k,i}$ is the wavelet component of ω_k at i^{th} wavelet level.

RESULTS AND DISUCUSSIONS

The spectra of the velocity signals u_2, measured on the vortex center for the free stream velocities of 4 m/s, 8 m/s and 12 m/s are shown in Figure 2, which exhibit strong peaks at frequencies f_0 of 140 Hz, 140 Hz and 190 Hz, respectively. The peaks become more apparent as Re increases. These frequencies correspond to a Strouhal number of about 0.2, which indicates a consequence of the occurrence of the large-scale structure of Kármán vortices. These corresponding shedding frequencies will therefore be used as the basic frequencies f_0 in the wavelet analysis to represent the large-scale vortical structures.

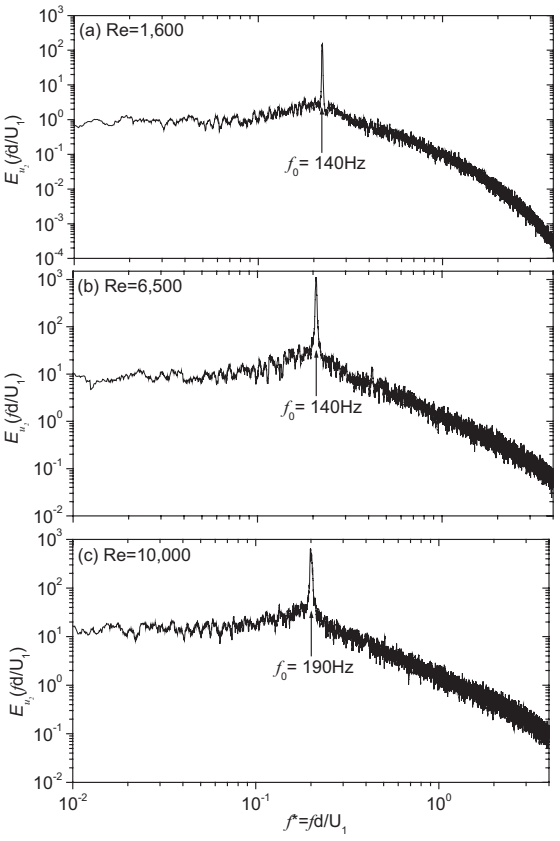

Figure 2 The u_2-spectrum

Contributions to Vorticity Variances from Different Wavelet Components at Re of 6,500

In this section, results and discussion will be focused on the measurements at the velocity of 8 m/s (i. e. Re = 6,500) to study the contributions to vorticity variances from different wavelet components. The wavelet multi-resolution technique was used to decompose the three vorticity components into a number of orthogonal wavelet vorticity components by $\omega_{k,i}$ where k represents the vorticity components in the x_1-, x_2-, and x_3-direction at the ith wavelet level. The wavelet level is based on the shedding frequency f_0, which represent the large-scale structures in wavelet analysis, as basic frequency to multiple by a factor of 1/2, 2, 4, 8, 16 and 32 ($\equiv f_0/2$, $2f_0$, $4f_0$, $8f_0$, $16f_0$ and $32f_0$) for the wavelet analysis of the various scale of turbulent structures. Then the vorticity variances of the wavelet components, $<\omega_k^2>_i$, may be calculated by $<\omega_k^2>_i = \frac{1}{n}\sum_{j=1}^{n}\omega_{j,k,i}^2$,where n is the total number of data points.

The distributions of the time-averaged three vorticity variances obtained from the wavelet multi-resolution analysis at different wavelet levels or central frequencies are shown in Fig. 3. The values of $<\omega_k^2>_i$ are normalized by the maximum measured value of $<\omega_k^2>_{\max}$ to indicate the contribution from different central frequencies to the vorticity variance, where k ($\equiv$ 1, 2 or 3) represents any component of the vorticity vector and $<\omega_k^2>_i$ represent the wavelet components at i^{th} level. The measured vorticity variances $<\omega_k^2>$ are also included in the figure for comparison. It can be seen in each figure that, both $<\omega_k^2>/<\omega_k^2>_{\max}$ and $<\omega_k^2>_i/<\omega_k^2>_{\max}$ drop when the free stream is approached. It needs to be noted that the maximum value of $<\omega_1^2>_i/<\omega_1^2>_{\max}$, corresponding to central frequency of f_0 (Fig. 3a), accounts for about 12.3% of the maximum longitudinal vorticity variance. This value is much larger than that for $<\omega_2^2>_i/<\omega_2^2>_{\max}$ (6.5%, Fig. 3b) and $<\omega_3^2>_i/<\omega_3^2>_{\max}$ (8.9%, Fig. 3c), indicating a relatively larger contribution to the longitudinal total vorticity variance from the large-scale structures than both to the transverse and to the spanwise vorticity components. This result seems to suggest that as the vortical structures evolve downstream, the spanwise and rib-like structures found in Rinoshika and Zhou (2005) show different contributions to the three vorticity components. Figure 3 also shows that the turbulent structures with higher central frequencies tend to contribute more to the vorticity variances than those of lower ones since $<\omega_1^2>_i/<\omega_1^2>_{\max}$ is largest at $4f_0$, while the contributions to $<\omega_2^2>_i/<\omega_2^2>_{\max}$ and $<\omega_3^2>_i/<\omega_3^2>_{\max}$ are dominated by structures with central frequency of $8f_0$. In Figs. 3b and c, it can be seen that contributions at $2f_0$, $4f_0$, 8 f_0 and 16 f_0 are all higher than that corresponding to f_0. The total contribution from the

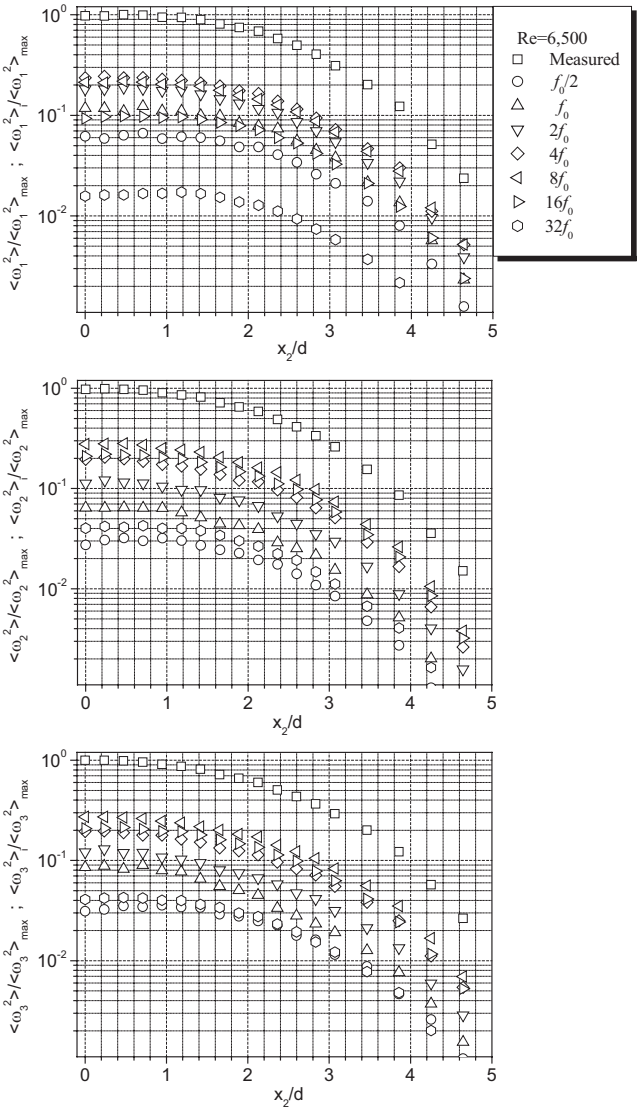

Figure 3 Vorticity variances of the measured and the wavelet components at various central frequencies for Re = 6,500

included subsets (2~32 f_0) takes about 76% of $<\omega_1^2>_{\max}$, 87% of $<\omega_2^2>_{\max}$ and 85% of $<\omega_3^2>_{\max}$, indicating that more transverse and spanwise vorticity resides in the intermediate and small-scale structures than the longitudinal vorticity component. In addition, this result is consistent with the previous study (Rinoshika and Zhou, 2005) that compared with the large-scale turbulent structures (with central frequencies lower than $2f_0$), the intermediate and relatively small-scale structures contribute more to vorticity.

Reynolds Number Effect on the Contributions to Vorticity Variances from Different Wavelet Components

Figure 4 shows the vorticity variances of the wavelet components at the central frequencies $f_0/2$, f_0, $2f_0$, $4f_0$, $8f_0$ and $16f_0$. The structures with central frequencies of $f_0/4$ and $32f_0$ contribute least to the total energy with a percentage

being smaller than 4%. Figure 4a shows the vorticity variances from the wavelet components at the central frequencies of $f_0/2$ and f_0, which represent the large-scale structures. Similar variations with *Re* are found for individual vorticity component and the wavelet contributions decrease with the increase of *Re*. The contribution of *Re*=1,600 to $\langle\omega_1^2\rangle$ from f_0 is largest, accounting for 21%.

The contributions to vorticity variances from structures with central frequencies of $2f_0$ and $4f_0$, which mainly represent the intermediate scale turbulent structures, are shown in Fig.4b. It can be seen that, the contributions at $2f_0$ decrease from 26% to 14% to $\langle\omega_1^2\rangle$, from 26% to 10% to $\langle\omega_2^2\rangle$ and $\langle\omega_3^2\rangle$, respectively, when *Re* increases. At central frequency of $4f_0$, the decrease of contributions is from 29% to 16% for $\langle\omega_3^2\rangle_i$ and $\langle\omega_2^2\rangle_i$. In contrast to $\langle\omega_3^2\rangle_i$ and $\langle\omega_2^2\rangle_i$, the decreases of $\langle\omega_1^2\rangle_i$ is smaller, and the contribution is from 22% to 20%. However, the contribution of *Re*=6,500 to $\langle\omega_1^2\rangle$ from $4f_0$ becomes larger than that of two *Re* numbers.

The contributions to vorticity variances at central frequencies of $8f_0$ and $16f_0$, which mainly represent the small-scale structures, are shown in Fig.4c significant increases or jump of contributions to the three vorticity components are observed when *Re* increases, indicating a strong positive *Re* dependence over the present *Re* range (1,600~10,000). In Fig.4c ($8f_0$), the increase of the contribution to $\langle\omega_1^2\rangle$ is from 7.5% to 24%, and the contributions of *Re*=6,500 to $\langle\omega_2^2\rangle$ and $\langle\omega_3^2\rangle$ become larger than that of two *Re* numbers, accounting for 28%. However, the corresponding increases are most significant at $16f_0$, which are from 1% to 19% for $\langle\omega_1^2\rangle_i/\langle\omega_1^2\rangle_{\max}$, from 1% to 30% for $\langle\omega_2^2\rangle_i/\langle\omega_2^2\rangle_{\max}$ and $\langle\omega_3^2\rangle_i/\langle\omega_3^2\rangle_{\max}$, when *Re* increases. Figure 5 exhibits the maxmimum vorticity variances of the wavelet components at different central frequencies. With the caveat of the experimental uncertainty associated with vorticity measurements, the changes of the wavelet contributions when Reynolds number is increased are still appreciable. This sudden "jump" of the contributions to vorticity variances from the turbulent structures with the central frequencies of $8f_0$ and $16f_0$ is probably due to the generation of small-scale structures in the near field. This result indicates that the vorticity field in the wake depends not only on the initial conditions, but also on the Reynolds numbers, which reveals the "memory" effects to the Reynolds number change in the near field.

CONCLUSIONS

All three components of the vorticity vector in the near region of a cylinder wake were measured simultaneously by employing an eight hot-wire probe at three Reynolds numbers, namely 1,000, 6,500 and 10,000. Using the wavelet multi-resolution technique, contributions to vorticity variances from different wavelet components are evaluated. It is found that the dominant contributions to the vorticity variances are from the intermediate and relatively small-scale structures. The contributions from the large and intermediate-scale structures to the vorticity variances decrease with the increase of Reynolds number, while the contributions from the small-scale structures to all three vorticity variances jump significantly. The result reinforces the conception that turbulence 'remembers' its origin.

REFERENCES

Lin J. C., Towfighi J. and Rockwell D,, 1995, "Instantaneous structure of the near-wake of a circular cylinder: on the effect of Reynolds number", *Journal of Fluids and Structures*, Vol.9, pp.409-418.

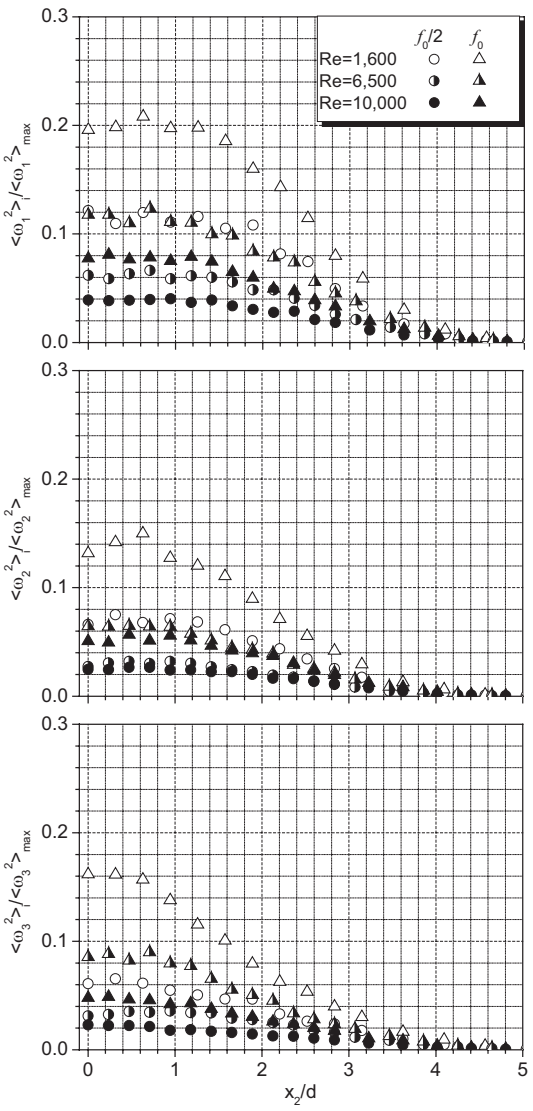

(a) $f_0/2$ and f_0

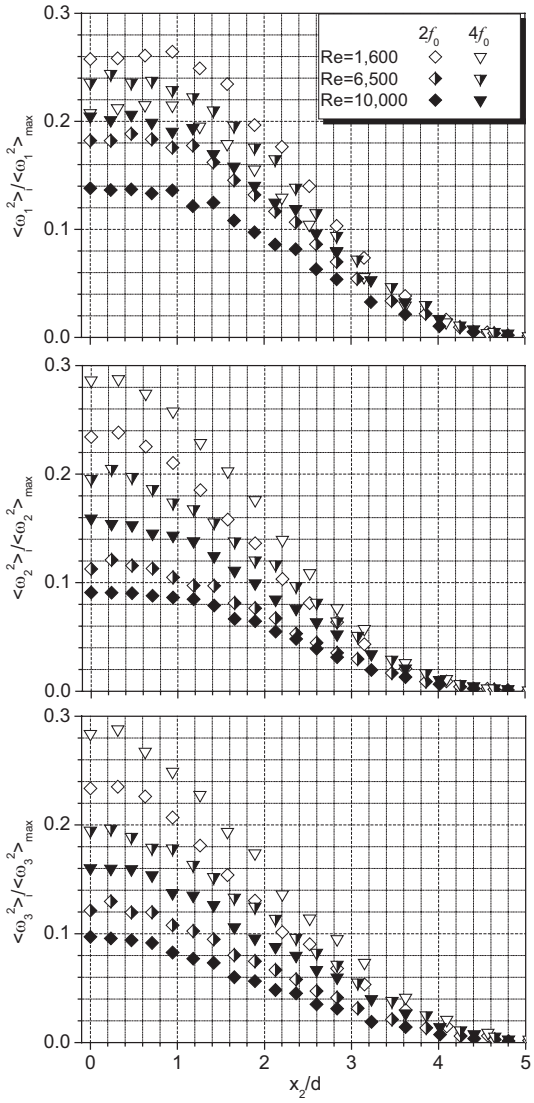

(b) $2f_0$ and $4f_0$

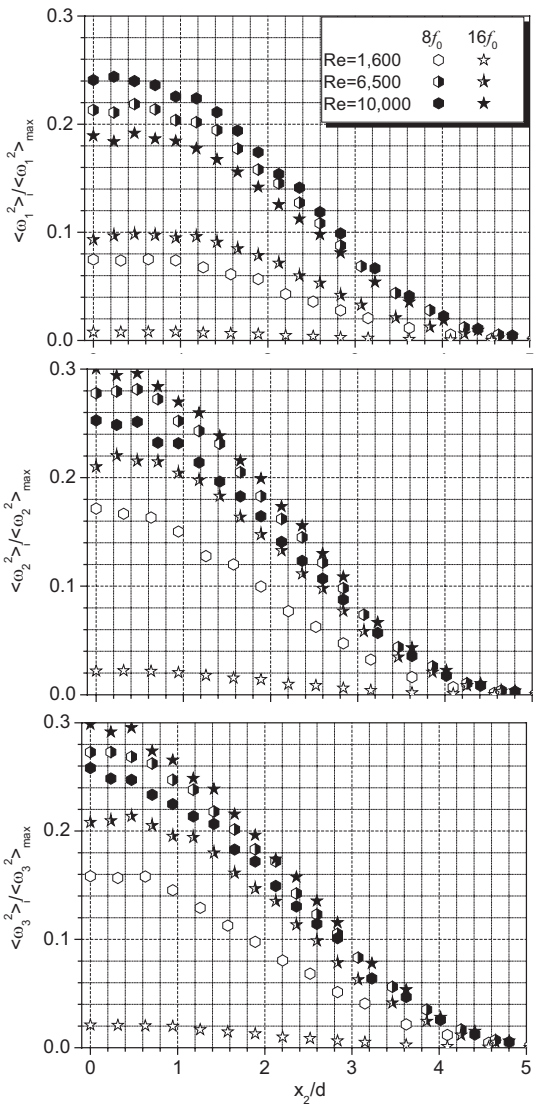

(c) $8f_0$ and $16f_0$

Figure 4 Vorticity variances of the wavelet components at various central frequencies

Yiu M. W., Zhou Y., Zhou T. and Cheng L., 2004, "Reynolds number effects on 3-D vorticity in a turbulent wake", *AIAA Journal*, Vol.42, pp.1009-1015.

Rinoshika A. and Zhou Y., 2005 "Orthogonal Wavelet Multi-Resolution Analysis of a Turbulent Cylinder Wake", *Journal of Fluid Mechanics*, Vo.524, pp.229-248.

Rinoshika A. and Zhou Y., 2005, "Effects of Initial Conditions on a Wavelet-decomposed Turbulent Near-wake", *Physical Review E*, Vol.71, 046303, pp.1-8.

Rinoshika A. and Zhou Y., 2007, "Effects of Initial Conditions on Wavelet-Decomposed Self-Preserving Turbulent Structures", *International Journal of Heat and Fluid Flow*, Vol.28, pp.948–962.

Zhou T., Rinoshika A., Hao Z., Zhou Y. and Chua L. P., 2006, "Wavelet multi-resolution analysis of the three vorticity components in a turbulent far wake", *Physical Review E*, Vol.73, 036307, pp.1-12.

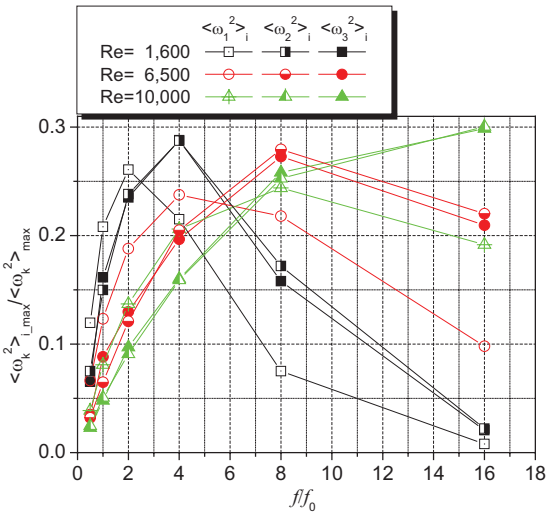

Figure 5 Maxmimum vorticity variances of the wavelet components for different central frequencies